Mater. Res. Soc. Symp. Proc. Vol. 1454 © 2012 Materials Research Society
DOI: 10.1557/opl.2012.1443

Ultraviolet (UV) photodetectors fabricated from multi-walled carbon nanotubes (MWCNTs) and polyvinyl-alcohol (PVA) coated ZnO nanoparticles

Dali Shao[a], Liqiao Qin[a,] and Shayla Sawyer[a]

[a]*Electrical, Computer, and Systems Engineering, Rensselaer Polytechnic Institute, USA, shaod@rpi.edu*

Abstract

Enhanced near band-edge (NBE) emission was observed from composite structures fabricated from a PVA coated ZnO (PVA-ZnO) nanoparticle thin film embedded with multi-walled carbon nanotubes (MWCNTs). The enhancement is attributed to the resonant coupling between the bandgap transition of the semiconductor and the surface plasmon (SP) of MWCNTs. Moreover, the PVA-ZnO/MWCNTs/PVA-ZnO composite structures show faster transient response, which is due to the carrier transportation process in the composite structure. Reductions are observed for both photocurrent to dark current ratio and intensity of photoresponsivity, demonstrating a tradeoff between the time transient response and the detectivity.

Introduction

ZnO is a wide band gap semiconductor material and has attracted extensive research effort due to the wide range of promising applications, including: field effect transistors (FET) [1-3], gas sensing [4-6] and optoelectronic devices [7-9]. Recently, ZnO based composite structures have received much attention because they can tune or improve material properties that are not easily achievable by using ZnO alone. For example, strongly enhanced UV emissions are observed for metal/ZnO composite structures, which are mainly due to the surface plasmon resonance (SPR) effect [10-12]. This effect is also demonstrated for graphene/ZnO and single-walled carbon nanotubes (SWCNTs)/ZnO composite structures [13-14]. Moreover, MWCNTs/ZnO composite structure show not only enhanced UV emission, but also improved the transient photoresponse [15-16]. However, to our knowledge, a systematic analysis of both the material and device properties for a MWCNTs/ZnO nanoparticle composite structure has not been studied. Therefore, here we report UV photodetectors employing PVA-ZnO/MWCNTs/PVA-ZnO composite structures with various parameters of the embedded MWCNT. The composite structures show enhanced UV emission, faster transient photoresponse, but a reduced photocurrent to dark current ratio and reduced photoresponsivity.

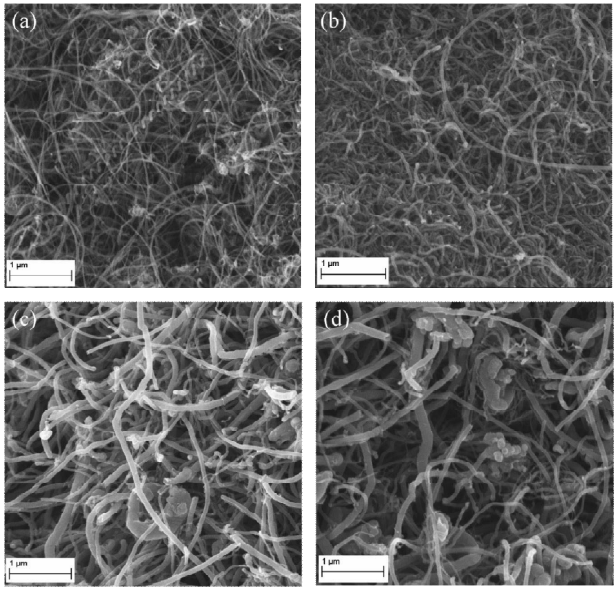

Figure 1. High resolution SEM image of multi-walled carbon nanotubes (MWCNTs) with different average external diameters: (a) 15nm, (b) 25nm, (c) 40nm, and (d) 65nm

Experiment

The ZnO nanoparticles used in this study are made by a top-down wet-chemical etching method [17]. The average diameter of the PVA-ZnO nanoparticles is 150 nm. The steps used to fabricate the PVA-ZnO/MWCNTs/PVA-ZnO composite structure are as follows. First, the PVA-ZnO nanoparticles were dispersed in ethanol to form a 30 mg/ml suspension. Then the solution was spin-coated onto quartz substrate and annealed in air at 120℃ for 5 min. In four separate solutions, uniform MWCNT suspensions were made by dispersing 10 mg of MWCNT (purchased from US Research Nanomaterials, Inc) with average external diameters varying from 15nm to 65 nm in 50ml ethanol. Each solution was sonicated for 1 hour. The MWCNTs were then spin-coated on top of four identical samples of PVA-ZnO nanoparticle thin film. The thickness of the MWCNTs network was controlled by changing the number of coatings. Finally, another 5 layers of PVA-ZnO nanoparticles thin film was deposited on top of the MWCNTs network. The high resolution SEM images of MWCNTs with different external diameters are shown in figure 1 and the schematic view of the composite structure is shown in figure 2.

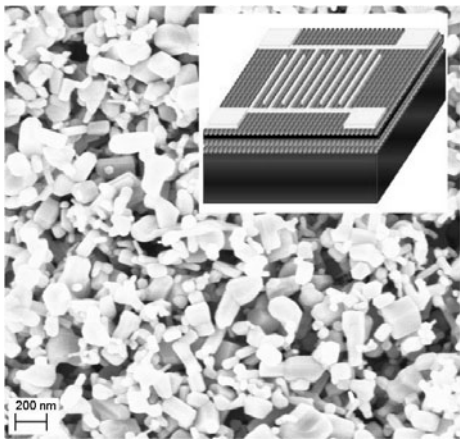

Figure 2. High resolution SEM image of PVA coated ZnO nanoparticles. The inset is the 3D view of photoconductor fabricated from PVA-ZnO/MWCNTs/PVA-ZnO composite structure with interdigitated aluminum contacts.

The following characterization methods were used to determine the material and optical characteristics of the PVA-ZnO/MWCNTs/PVA-ZnO composite structure. A Carl Zeiss Ultra 1540 dual beam scanning electron microscope (SEM) was used to determine morphology of the MWCNTs and PVA-ZnO nanoparticles. Photoluminescence (PL) spectra were measured using a Spex Fluoro log Tau-3 spectrofluorimeter. Transient current response and photocurrent to dark current ratio were measured using a HP4155B semiconductor parameter analyzer. All measurements were performed at room temperature in air.

Results and Discussions

Figure 3 illustrates the room temperature PL spectra measured for different samples of PVA-ZnO with 10 layers of MWCNTs. Each sample has MWCNT with a specific external diameter. The first peak around 380 nm is due to NBE recombination while the second peak around 540 nm originates from deep defect levels induced by oxygen vacancy defects [18-20]. The enhancement factor is defined as the ratio of the intensity of PL peak for the composite structure samples to that of the PL peak for reference sample of bare PVA-ZnO. The enhancement factor for NBE recombination (white pillar) and defect level emission (dark pillar) is presented in the inset of figure 3. Surface plasmon resonance (SPR) is the cause of PL enhancement. In the interface of the MWCNTs/PVA-ZnO nanoparticles, the SP frequency is determined by [14, 15] [21]:

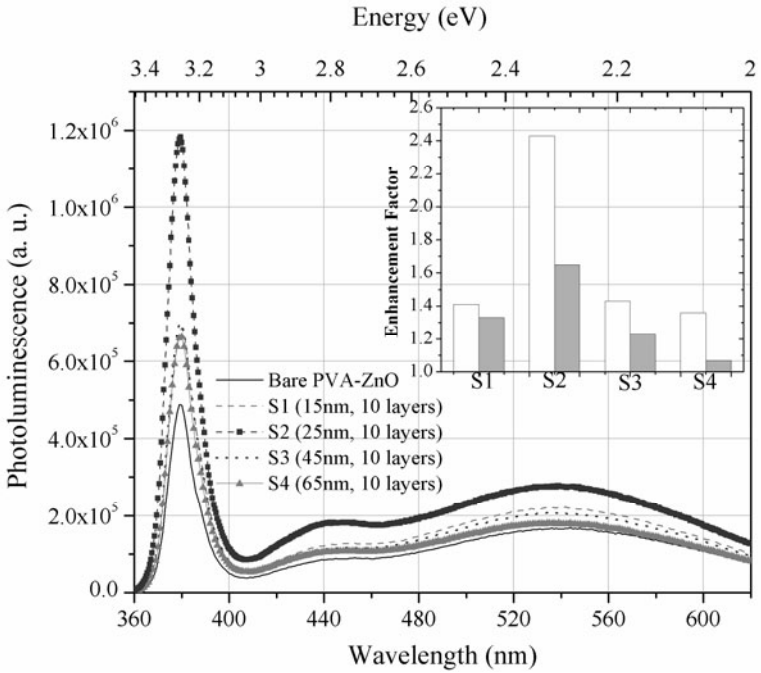

Figure 3. Room temperature PL measured of thin films fabricated with CNTs/PVA-ZnO composite structure and from bare PVA-ZnO nanoparticles. The inset shows the enhancement factors for the two bands (One with a peak wavelength at 380 nm and the other with a peak wavelength at 540 nm) in the PL spectra. Inset: The gray and yellow bars represent enhancement factors for the 380 nm band and 540nm band respectively.

$$\omega_{sp} = \frac{\omega_p}{\sqrt{1+\varepsilon_2}}$$

Where ω_p is the bulk plasmon frequency and ε_2 is the dielectric constant of the medium below the MWCNTs. In the concept device shown in Figure 2, we can assume that due to the inherent nature of the interface between the MWCNTs and ZnO nanoparticle there are gaps causing the MWCNTs to be in direct contact with air. So the dielectric constant of the medium, ε_2, can be taken to be 1 and ω_{sp} can be reduced to:

$$\omega_{sp} = \frac{\omega_p}{\sqrt{2}}$$

The bulk plasma frequency of a CNT bundle is given by [14]:

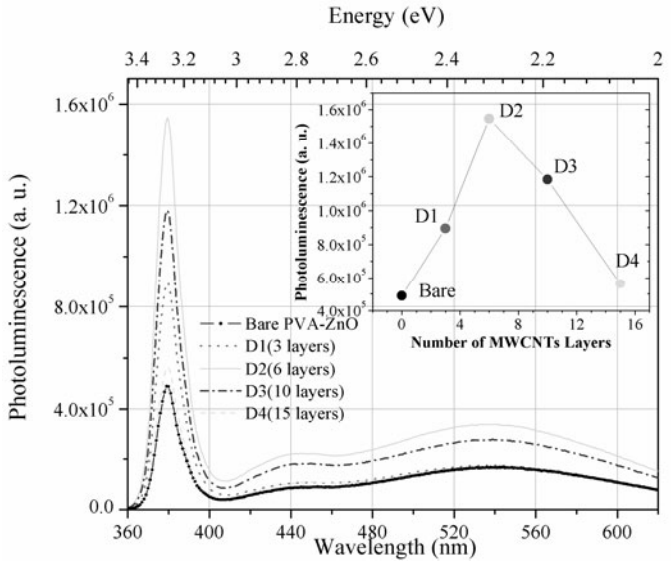

Figure 4. Room temperature PL measured for composite structures with varying thickness of MWCNTs with external diameter of 25 nm. The inset is peak intensity of the PL versus the number of MWCNTs layers embedded in the composite structure.

$$\omega_p = \frac{q_z}{q}\sqrt{\frac{4\pi e^2 n_{mw}}{\varepsilon_1 m^*}}$$

Where q_z is the wave-vector component along the MWCNTs, n_{mw} is the free electron density, $\varepsilon_1=2.4\varepsilon_0$ is the background dielectric constant of MWCNTs and ε_0 is the dielectric constant of free space and m^* is the effective electron mass. The MWCNTs can be regarded as one dimensional conductor and therefore q_z/q =1 and free electrons mass are used for m^*. The MWCNTs can be viewed as concentric structures with many single walled carbon nanotubes (SWCNT). Therefore, the free electron density of the MWCNTs can be calculated by:

$$n_{mw} = \sum_{n=1}^{n} \frac{8}{\sqrt{3}\pi a}\frac{1}{(d_n)^2}$$

In this expression, a = 0.249 nm is the lattice constant of the graphite sheet, n is the number of SWCNTs in each MWCNT and d_n is the diameter of the concentric SWCNTs. The distance between each wall of the concentric SWCNT is 0.34 nm and the diameter of the inner SWCNT for S1-S4 is 7.5nm, 7.5nm, 8.5nm and 10nm, respectively (Parameters obtained from US Research Nanomaterials, Inc). n is calculated to be 11, 26, 46, 81 for S1-S4, respectively. By

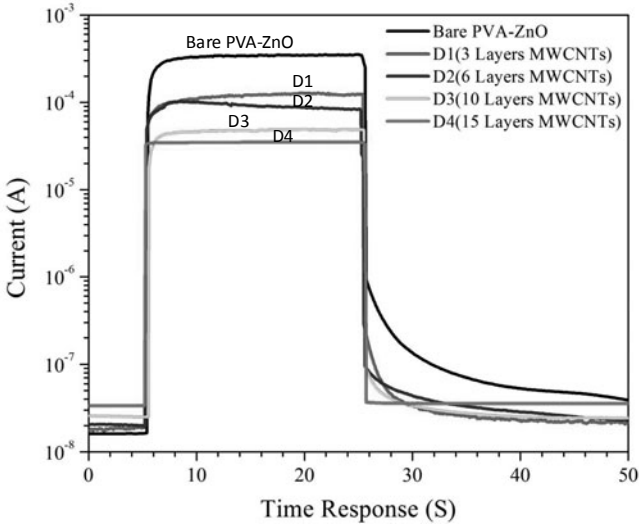

Figure 5. Transient photocurrent of the bare PVA-ZnO and PVA-ZnO/MWCNTs/PVA-ZnO composite structures.

substituting these parameters into the above equations, we get the SPR frequencies for S1 to S4 are: 3.97eV, 3.60eV, 2.87eV and 2.12eV, respectively. The calculated value of resonance frequency for S2 is close to the band gap of ZnO (3.3eV), which explains the best coupling effect observed for S2 compared with the S1, S3 and S4.

Figure 4 represents room temperature PL spectra as a function of number of MWCNTs layers for composite structures with MWCNTs with average external diameters of 25 nm. The number of MWCNTs layers range from 3 to 15 layers, which correspond to sample D1 to D4 respectively. The highest PL peak intensity was observed for sample D2. Increasing the number of MWCNTs layers beyond 6 layers reduces the PL peak intensity. This is likely due to the blocking of UV light with increasing layers which reduces the amount of light that can be absorbed by the PVA-ZnO layer.

The time resolved photocurrent measured for bare PVA-ZnO and the composite structures (D1-D4) with varying number of coatings of MWCNTs layers are presented in Figure 5. The rise time can be represented by $I = I_0(1 - e^{-t/\tau_r})$ while the fall time follows $I = I_0(e^{-t/\tau_{f1}} + e^{-t/\tau_{f2}})$. Where τ_r is the rise time constant, τ_{f1} correspond to the initial fast change of the fall time and τ_{f2} represents the slow tails of the fall time. By fitting the above expression with the measured rise time and fall time curves, τ_r, τ_{f1} and τ_{f2} have been determined and are listed in Table 1. It shows that the PVA-ZnO/MWCNTs/PVA-ZnO composite structures have faster rise times and fall times than bare PVA-ZnO.

Table 1. The value of photocurrent to dark current ratio, rise and fall time constants of the bare PVA-ZnO and PVA-ZnO/MWCNTs/PVA-ZnO composite structures.

Sample	I_{ph}/I_d	τ_r(s)	τ_{f1}(s)	τ_{f2}(s)
Bare PVA-ZnO	2.2×10^3	1.41s	0.25s	7.57s
D1	6.9×10^2	0.74s	0.12s	5.67s
D2	5.0×10^2	1.01s	0.17s	6.38s
D3	2.1×10^2	0.64s	0.10s	5.46s
D4	1.1×10^2	0.42s	0.05s	2.04s

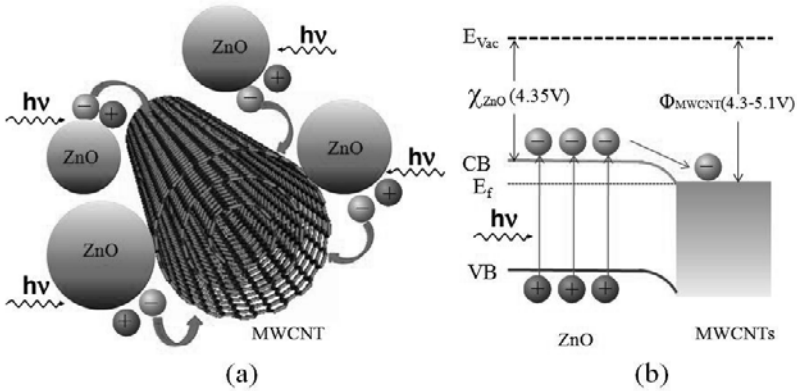

Figure 6. (a) Carrier transportation process and (b) Energy band diagram for PVA-ZnO/MWCNTs/PVA-ZnO composite structure.

The improved transient photoresponse can be understood from the carrier transportation process and energy band diagram of the composite structure is shown in figure 6 (a) and (b). Due to the semi-metallic property of the MWCNTs, [22] the composite structure are expected to have better conductivity than the bare PVA-ZnO film. The electron affinity for ZnO is 4.35eV [15] and the Fermi level of the MWCNT is known to be 4.3–5.1 eV [23] below the vacuum level. Thus, when ZnO contact with the MWCNTs, it is energetically favorable for the electron to transfer from the ZnO to the MWCNTs. With UV illumination, the photogenerated electrons reach the ZnO conduction band and then transfer to the MWCNTs. Since MWCNTs are semi-metallic and

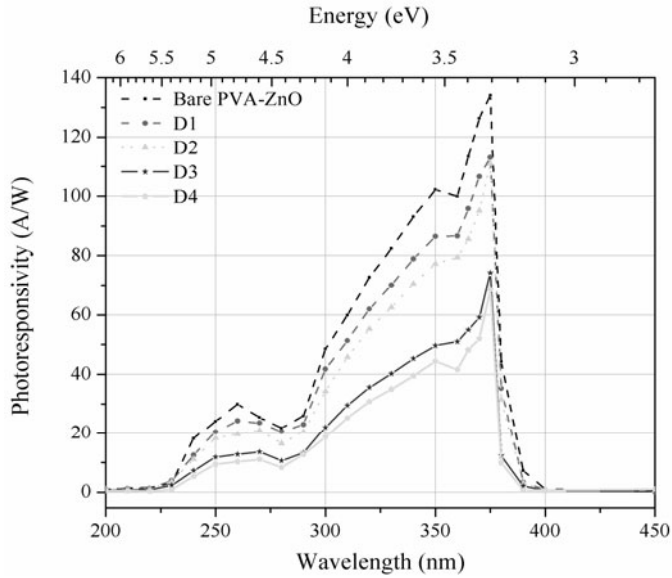

Figure 7. Photoresponsivity spectra measured for photodetectors fabricated from bare PVA-ZnO and from the composite structures embedded with different number of MWCNTs layers.

have better conductivity, there is less accumulation of the electrons on CNTs side. This enhances the electron–hole separation and improves carrier transportation in the composite structure, leading to a faster rise of the photocurrent. When UV illumination is turned off, the excess electrons in the MWCNTs side transfer to the ZnO side for recombination with holes which is a very fast process [15] [24], and thus the decay is faster than the bare PVA-ZnO nanoparticles.

Although the PVA-ZnO/MWCNTs/PVA-ZnO composite structure proved to enhance PL emission and give a faster time response, the photocurrent to dark current ratio decreases as the thickness of the MWCNTs layers increase. This can be explained by two possible mechanisms. First, the reduced ratio can be attributed to increased dark current while the photocurrent is reduced. The increased dark current is due to the semi-metallic properties of the MWCNTs, which improved the conductivity of the composite structure. Yet, with increased number of the MWCNTs layers, less UV light can reach to the bottom PVA-ZnO layers, leading to a reduction in the number of photogenerated carriers. Second, it is well known that the oxygen molecules adsorb onto the surface of ZnO nanoparticles and capture nearby electrons to form an O_2^- layer $[O_2(g)+e^- \rightarrow O_2^-(ad)]$, which leads to a formation of a space charge region near the surface of ZnO. Upon exposure to the UV light, the photogenerated holes will recombine with oxygen ions formed on the surface of ZnO nanoparticles $[h^+ + O_2^-(ad) \rightarrow O_2(g)]$, resulting in a decrease in the

width of the depletion region. Thus, the space charge region effect contributes to photoconductive gain of ZnO nanoparticles. Due to the high surface to volume ratio, this effect can be significant for ZnO nanoparticles. However, after introducing the MWCNTs, the photogenerated carriers are likely to transfer to the MWCNTs side without reacting with the space charge region, as shown in figure 6 (a). Thus the space charge region effect is weakened, leading to reduced photoconductive gain for ZnO nanoparticles. In sum, there is a tradeoff between time response and photocurrent to dark current ratio. This conclusion is further supported by the photoresponsivity measurement, as shown in figure 7. The intensity of the photoresponsivity spectra decreases as the number of the MWCNTs layers increase, which agrees with the results shown in the transient response measurement. Two major peaks are observed, which are located at 375nm and 260nm, respectively. The first peak (375nm) is due to the band edge transitions in the ZnO nanoparticles while the second peak (260nm) origin is unclear and still under investigation.

Conclusion

In conclusion, UV photodetectors were fabricated from PVA-ZnO/MWCNTs/PVA-ZnO composite structures which show enhanced band edge emission and faster transient photoresponse. These enhancements are due to the SPR effect and the transfer of carriers from ZnO to the semi-metallic MWCNTs, respectively. The photocurrent to dark current ratio and photoresponsivity decreases as the number of MWCNTs layers increase, explained as the blocking of UV light of the MWCNTs layers from the PVA-ZnO layer.

Acknowledgement

The authors gratefully acknowledge support from National Security Technologies through NSF Industry/University Cooperative Research Center Connection One. The authors also acknowledge the National Science Foundation Smart Lighting Engineering Research Center (EEC-0812056).

References

[1] A. N. Shipway, E. Katz, and I. Willner, “Nanoparticle arrays on surfaces for electronic, optical and sensoric applications,” Chem. Phys. Chem. vol. 1, issue 1, pp. 18-52, Aug. 2000.

[2] F. Favier, E. C. Walter, M. P. Zach, T. Benter, and R. M. Penner, “Hydrogen Sensors and Switches from Electrodeposited Palladium Mesowire Arrays,” Science, vol. 293, no. 5538, pp. 2227-2231, Sep. 2001.

[3] C. Li, D. H. Zhang, X. L. Liu, S. Han, T. Tang, J. Han, and C. W. Zhou, “In_2O_3 nanowires as chemical sensors,” Appl. Phys. Lett. vol. 82, no. 10, pp. 1613-1615, Mar. 2003.

[4] G. Korotcenkov, A. Cerneavschi, V. Brinzari, A. Vasiliev, M. Ivanov, A. Cornet, J. Morante, A. Cabot, and J. Arbiol, “In_2O_3 films deposited by spray pyrolysis as a material for ozone gas

sensors," Sens. Actuators B: Chem. vol. 99, issue 2-3, pp. 297, May 2003.
[5] M. Ivanovskaya, A. Gurlo, and P. Bogdanov, "Mechanism of O3 and NO2 detection and selectivity of In2O3 sensors," Sens. Actuators B: Chem. vol. 77, issue 1-2, pp. 264-267, June 2001.
[6] A. Z. Sadek, C. Baker, D. A. Powell, W. Wlodarski C. Shin, R. B. Kaner, and K. Kalantar-zadeh, "A Polyaniline/In_2O_3 Nanofiber Composite Based Layered SAW Transducer for Gas Sensing Applications," Nanotechnology, vol. 17 (17) , pp. 4488-4492, 2006..
[7] L. C. Chen, "Indium oxide violet photodiodes," Phys. Eur. Phys. J. Appl. Phys. 35: 13–15, July 2006.
[8] K. L. Chopra, S. Major, and D. K. Pandya, Thin Solid Films, vol. 102, issue 1, pp.1-46, 1983.
[9] D. S. Ginley and C. Bright, "Transparent conducting oxides," Mater. Res. Soc. Bull. 25, pp. 15-18, 2000.
[10] X. H. Xiao, F. Ren, X. D. Zhou, T. C. Peng, W. Wu, X. N. Peng, X. F. Yu, and C. Z. Jiang, "Surface plasmon-enhanced light emission using silver nanoparticles embedded in ZnO," Appl. Phys. Lett. vol. 97, 071909, 2010.
[11] W. H. Ni, J. An, C. W. Lai, H. C. Onga and J. B. Xu, "Emission enhancement from metallodielectric-capped ZnO films," Appl. Phys. Lett. 100, 026103, 2006.
[12] K. Wu, Y. Lu, H. He, J. Huang, B. Zhao, and Z. Ye, "Enhanced near band edge emission of ZnO via surface plasmon resonance of aluminum nanoparticles," Appl. Phys. Lett. 110, 023510, 2011.
[13] S. W. Hwang, D. H. Shin, C. O. Kim, S. H. Hong, M. C. Kim, J. Kim, K. Y. Lim, S. Kim, Suk-Ho Choi, K. J. Ahn, G. Kim, S. H. Sim, and B. H. Hong, "Plasmon-Enhanced Ultraviolet Photoluminescence from Hybrid Structures of Graphene/ZnO Films," Phys. Rev. Lett. 105, 127403 (2010).
[14] S. Kim, D. H. Shin, C. O. Kim, S. W. Hwang, Suk-Ho Choi, S. Ji, and Ja-Yong Koo, Appl. Phys. Lett. 94 (2009) 213113.
[15] M. Dutta, D. Basak, Chem. Phys. Lett 480 (2009) 253–257.
[16] Y. Zhu, H. I. Elim, Yong-Lim Foo, T. Yu, Y. Liu, W. Ji, Jim-Yang Lee, Z. Shen, A. Thye-Shen Wee, J. Thiam-Leong Thong, and Chorng-Haur Sow, "Multiwalled Carbon Nanotubes Beaded with ZnO Nanoparticles for Ultrafast Nonlinear Optical Switching," Adv. Mater., 18, 587–592, 2006.
[17] L. Qin, C. Shing, S. Sawyer, and P. S. Dutta, Opt. Mater. 33 (2011) 359-362.
[18] S. Monticone, R. Tufeu, A. Kanaev, J. Phys. Chem. B 102 (1998) 2854.
[19] Y. Wu, A. Tok, F. Boey, X. Zeng, X. Zhang, Appl. Surf. Sci. 253 (2007) 5473.
[20] L. Wu, Y. Wu, X. Pan, F. Kong, Opt. Mater. 28 (2006) 418.
[21] H. Raether, Excitation of Plasmons and Interband Transitions by Electrons, Springer, New York, 1980.
[22] Nanostructured Materials and Nanotechnology, Academic Press, New York,2002
[23] H. Ago, T. Kugler, F. Cacialli, W.R. Salaneck, M.S.P. Shaffer, A.H. Windle, R.H.Friend, J. Phys. Chem. B 103 (1999) 8116.
[24] I. Robel, B.A. Bunker, P. V. Kamat, Adv. Mater. 17 (2005) 2458.